ADAPTIVE DATA-DRIVEN REGULARIZATION FOR VARIATIONAL IMAGE RESTORATION IN THE BV SPACE

Hongwei Zheng and Olaf Hellwich
Computer Vision & Remote Sensing, Berlin University of Technology
Franklinstrasse 28/29, Sekretariat FR 3-1, D-10587 Berlin

Keywords: Bayesian estimation, regularization, convex optimization, functions of bounded variation, linear growth functional, self-adjusting, parameter estimation, data-driven, hyperbolic conservation laws, image restoration.

Abstract: We present a novel variational regularization in the space of functions of Bounded Variation (BV) for adaptive data-driven image restoration. The discontinuities are important features in image processing. The BV space is well adapted for the measure of gradient and discontinuities. More over, the degradation of images includes not only random noises but also multiplicative, spatial degradations, i.e., blur. To achieve simultaneous image deblurring and denoising, a variable exponent linear growth functional on the BV space is extended in Bayesian estimation with respect to deblurring and denoising. The selection of regularization parameters is self-adjusting based on spatially local variances. Simultaneously, the linear and non-linear smoothing operators are continuously changed following the strength of discontinuities. The time of stopping the process is optimally determined by measuring the signal-to-noise ratio. The algorithm is robust in that it can handle images that are formed with different types of noises and blur. Numerical experiments show that the algorithm achieves more encouraging perceptual image restoration results.

1 INTRODUCTION

The primary goal of image restoration is to recover lost information from a degraded image and obtain the best estimate to the original image. Its applications include photography, remote sensing, medical imaging, and multimedia processing. According to the image degradation model $g = hf + \eta$, given an observed image function $g \in L^2(\Omega)$, with $\Omega \subset \mathbb{R}^2$ is an open bounded domain, the problem is to estimate the original image f with unknown noise η and point spread function h. In order to solve this ill-posed inverse problem, one of the well-known techniques is by energy minimization and regularization.

In classical Sobolev spaces, we can not make detailed analysis and reasonable measure of discontinuities. A simple image including a white disk on a black background is not in any Sobolev space, but belongs to the BV space. The BV space is the space of functions for which the sum of the perimeters of the level sets is finite. Therefore, the BV space is well adapted for determining discontinuities across or along edges. Compared to wavelet based methods in the frequency domain (Gousseau and Morel, 2001), the assumption of the functions on the BV space is still too restrictive to represent tiny detailed textures and infinite discontinuities (Alvarez and Gousseau, 1999). However, currently, the BV space is still a much larger space than the Sobolev space for modeling images in the spatial domain.

Since the seminal work of the ROF model (Rudin et al., 1992), the BV space based functionals have been widely applied to image restoration, super-resolution approaches, segmentation and related early vision tasks, e.g., Mumford-Shah functional (Mumford and Shah, 1989), modeling of oscillatory components (Meyer, 2001), modeling of inpainting and super-resolution approaches, (Chan and Shen, 2006). Recently, (Aubert and Vese, 1997), (Vese, 2001) propose a convex linear growth functional in the BV space for deblurring and denoising using Γ-convergence approximation. (Chen et al., 2006), (Chen and Rao, 2003) suggest a more general variable exponent, linear growth functional in the BV space

Zheng H. and Hellwich O. (2007).
ADAPTIVE DATA-DRIVEN REGULARIZATION FOR VARIATIONAL IMAGE RESTORATION IN THE BV SPACE.
In *Proceedings of the Second International Conference on Computer Vision Theory and Applications - IFP/IA*, pages 53-60

for image denoising. However, through the literature study, we find that only little work is done on how to determine regularization parameters, and diffusion operators for achieving optimal and high-fidelity image restoration results.

In this paper, we extend the variable exponent, linear growth functional (Chen et al., 2006), (Chen and Rao, 2003) to double regularized Bayesian estimation for simultaneously deblurring and denoising. The Bayesian framework provides a structured way to include prior knowledge concerning the quantities to be estimated (Freeman and Pasztor, 2000). Different from traditional "passive" edge-preserving methods (Geman and Reynolds, 1992), our method is an "active" data-driven approach which integrates self-adjusting regularization parameters and dynamic computed gradient prior for self-adjusting the fidelity term and multiple image diffusion operators. A new scheme is designed to select the regularization parameters adaptively on different levels based on the measurements of local variances. The chosen diffusion operators are automatically adjusted following the strengths of edge gradient. The suggested approach has several important effects: firstly, it shows a theoretically and experimentally sound way of how local diffusion operators are changed automatically in the BV space. Secondly, the self-adjusting regularization parameters also control the diffusion operators simultaneously for image restoration. Finally, this process is relatively simple and can be easily extended for other regularization or energy optimization approaches. The experimental results show that the method yields encouraging results under different kinds and amounts of noise and degradation.

The paper is organized as follows. In section 2, we discuss the concepts of BV space, the total variation (TV) model and its related functionals. In section 3, we present a Bayesian estimation based adaptive variational regularization with respect to the estimation of PSFs and images. Numerical approximation and experimental results are shown in section 4. Conclusions are summarized in section 5.

2 RELATED WORK

2.1 The Bv Space and the Tv Method

Following the total variation (TV) functional (Rudin et al., 1992), (Chambolle and Lions, 1997), (Weickert and Schnörr, 2001), (Chan et al., 2002), (Aubert and Vese, 1997), we study the total variation functional in the bounded total variation (BV) space.

Definition 2.1.1 *$BV(\Omega)$ is the subspace of functions $f \in L^1(\Omega)$ where the quantity is finite,*

$$TV(f) = \int_\Omega |Df|dA = \sup\left\{\int_\Omega f \cdot \mathrm{div}\varphi dA \; ; \; \varphi \in C_c^1(\Omega, \mathbb{R}^N)\right\} \quad (1)$$

where $dA = dxdy$, $|\varphi(A)|_{L^\infty(\Omega)} \leq 1$, $C_c^1(\Omega, \mathbb{R}^N)$ is the space of functions in $C^1(\Omega)$ with compact support Ω. $BV(\Omega)$ endowed with the norm $\|f\|_{BV(\Omega)} = \|f\|_{L^1(\Omega)} + TV(f)$ which is a Banach space.

While one adopts the TV measure for image regularization, the posterior energy for Tikhonov Regularization then takes the form which is also given in (Rudin et al., 1992),

$$\jmath(f) = \frac{\lambda}{2}\int_\Omega |g - hf|^2 dA + \int_\Omega |Df|dA \quad (2)$$

where g is the noisy image, f is an ideal image and $\lambda > 0$ is a scaling regularization parameter. When an image f is discontinuous, the gradient of f has to be understood as a measure. The $TV(f)$ functional is often denoted by $\int_\Omega |Df|dxdy$, with the symbol D referring to the conventional differentiation ∇. One use $f \in L^1(\Omega)$ to simplify the numerical computation (see (Giusti, 1984), for instance), $\int_\Omega |Df|dA = \int_\Omega |\nabla f|dA$.

In order to study more precisely the influence of the smoothing term in the regularization, we need to make an insight observation of a more general total variation functional which can help us to understand the convexity criteria in variational regularization. A general bounded total variational functional can be written in the following,

$$\jmath(f_{(g,h)}) = \frac{\lambda}{2}\int_\Omega (g - hf)^2 dA + \int_\Omega \phi(|\nabla f(x,y)|)dA$$

The choice of the function ϕ is crucial. It determines the smoothness of the resulting function f in the space $V = \{f \in L^2(\Omega); \nabla f \in L^1(\Omega)\}$ which is not reflexive.

In this variational energy function, the closeness of the solution to the data is imposed by the penalty term $\phi(\cdot)$ in the energy function. If the energy functions are nonconvex, it might become more complicated than the convex functionals. Although some non-convex $\phi(\cdot)$ penalty terms can achieve edge-preserving results, convex penalty terms can help us to get a global convergence and decrease the complexity of computation. In the following, we study $\phi(\cdot)$ in a more general form $\phi(\nabla f) \to \phi(Df)$ in the BV space.

2.2 Convex Linear-Growth Functional

Let Ω be an open, bounded, and connected subset of $\mathbb{R}^N$. We use standard notations for the Sobolev

$W^{1,p}(\Omega)$ and Lebesgue spaces $L^p(\Omega)$. A variational function can be written in the form,

$$\mathcal{J}(f_{(g,h)}) = \frac{\lambda}{2}\int_\Omega (g-hf)^2 dA + \int_\Omega \phi(Df(x,y))dA$$

where the function $\int_\Omega \phi(Df)dA$ is finite on the space $W^{1,1}$ which is a nonreflexive Banach space.

We recall the notation of lower semicontinuity of functionals defined on the $BV(\Omega)$ space. We denote by $\mathcal{L}_N$ the Lebesgue N-dimensional measure $\mathbb{R}^N$ and by $\mathcal{H}^\alpha$ the α-dimensional Hausdorff measure. We say that $f \in L^1(\Omega)$ is a function of bounded variation ($f \in BV(\Omega)$) if its distributed derivative $Df = (D_1 f, ..., D_N f)$ belongs to the weakest topology on $\mathcal{M}(\Omega)$. $\mathcal{M}(\Omega)$ is the set of all signed measures on Ω with bounded total variation.

For any function $f \in L^1(\Omega)$, we denote by S_f the complement of the Lebesgue set of f. The set S_f is of zero Lebesgue measure and is also called the *jump set of* f. If $f \in BV(\Omega)$, then f is differentiable almost everywhere on $\Omega \setminus S_f$. Moreover, the Hausdorff dimension of S_f is at most $(N-1)$ and for $\mathcal{H}^{N-1}$, $x \in S_f$ it is possible to find unique $f^+(x), f^-(x) \in \mathbb{R}$, with $f^+(x) > f^-(x)$ and $\nu \in S^{N-1}$ of unit sphere in $\mathbb{R}^N$, such that

$$\lim_{r\to 0^+} r^{-N}\int_{B_r^\nu(x)} |f(y)-f^+(y)|dy$$
$$= \lim_{r\to 0^+} r^{-N}\int_{B_r^\nu(x)} |f(y)-f^-(y)|dy = 0 \qquad (3)$$

where $B_r^\nu(x) = \{y \in B_r(x)\} : (y-x)\cdot\nu > 0$ and $B_r^{-\nu}(x) = \{y \in B_r(x)\} : (y-x)\cdot\nu < 0$. The normal ν means that they points toward the larger value in the image f. We denote by $B_r(x)$ the ball centered in x of radius r, shown in Fig. 1.

We have the Lebesgue decomposition,

$$Df = \nabla f \cdot \mathcal{L}_N + D^s f \qquad (4)$$

where $\nabla f \in (L^1(\Omega))^N$ is the Radon-Nikodym derivative of Df with respect to $\mathcal{L}_N$. In other words, ∇f is the density of the absolutely continuous part of Df with respect to the Lebesgue measure. We also have the decomposition for $D^s f = C_f + J_f$, where $J_f = (f^+ - f^-)N_f \cdot \mathcal{H}_S^{N-1}$ is *Hausdorff part* or *jump part* and C_f is the *Cantor part* of Df. The measure C_f is singular with respect to $\mathcal{L}_N$ and it is diffuse, that is, $C_f(S) = 0$ for every set S of Hausdorff dimension $N-1$. $\mathcal{H}_{|S_f}^{N-1}$ is called the perimeter of related edges in Ω. Finally, we can write Df and its total variation on Ω, $|Df|(\Omega)$, in the following,

$$Df = \nabla f \cdot \mathcal{L}_N + C_f + (f^+ - f^-)\nu \cdot \mathcal{H}_{|S_f}^{N-1}$$

$$|Df| = \int_\Omega |\nabla f|dx + \int_{\Omega\setminus S_f} |C_f| + \int_{S_f}(f^+ - f^-)d\mathcal{H}_{|S_f}^{N-1}$$

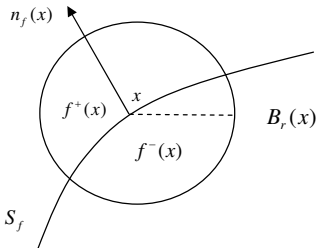

Figure 1: Definition of f^+, f^-, and the jump set S_f.

It is then possible to define the convex function of measure $\phi(|\cdot|)$ on $\mathcal{M}(\Omega)$, which is for Df,

$$\phi(|Df|) = \phi(|\nabla f|)\cdot\mathcal{L}_N + \phi^\infty(1)|D^s f|, \qquad (5)$$

and the functional following (Goffman and Serrin, 1964),

$$\int_\Omega \phi(|Df|) = \int_\Omega \phi(|\nabla f|)dx + \int_\Omega \phi^\infty(1)|D^s f|, \quad (6)$$

where the functional $\phi(|\cdot|)(\Omega)$ is proved in weak topology and lower semi-continuous on $\mathcal{M}(\Omega)$. That is to say that $\int_\Omega \phi(|Df|)$ is convex on $BV(\Omega)$, ϕ is convex and increasing on $\mathbb{R}^+$.

By the decomposition of $D^s f$, the properties of C_f, J_f, and the definition of the constant c, the functional $\int_\Omega \phi(|Df|)$ can be written as,

$$\begin{aligned}\int_\Omega \phi(|Df|) &= \int_\Omega \phi(|\nabla f|)dx \\ &+ c\int_{\Omega\setminus S_f} |C_f| + c\int_{S_f}(f^+ - f^-)d\mathcal{H}_{|S_f}^{N-1}\end{aligned}$$

Based on this equation, the energy functional on the BV space becomes,

$$\inf_{f\in BV(\Omega)} \mathcal{J} = \frac{\lambda}{2}\int_\Omega (g-hf)^2 dA + \int_\Omega \phi(|Df|)dA \quad (7)$$

Although some characterization of the solution is possible in the distributional sense, it remains difficult to handle numerically. To circumvent the problem, (Vese, 2001) approximates the BV solution using the notion of Γ-convergence which is also an approximation for the well-known Mumford-Shah functional (Mumford and Shah, 1989). The Mumford-Shah functional is a sibling of this functional (Chan and Shen, 2006).

The target of studying these functionals on the BV space is to understand a more general variable exponent, L^p linear growth functional which is a deduction functional on the BV space.

2.3 Variable Exponent Linear-Growth Functional

While the penalty function is $\phi(|Df|) \to \phi(x,|Df|)$, it becomes a variable exponent linear growth functional

in the BV space (Chen et al., 2006), (Chen and Rao, 2003),

$$\jmath(f_{(g,h)}) = \frac{\lambda}{2}\int_\Omega (g-hf)^2 dA + \int_\Omega \phi(x,Df(x,y))dA$$

For the definition of a convex function of measures, we refer to the works of (Goffman and Serrin, 1964), (Demengel and Teman, 1984). According to their work, for $f \in BV(\Omega)$, we have,

$$\int_\Omega \phi(x,Df)dA = \int_\Omega \phi(x,\nabla f)dA + \int_\Omega |D^s f|dA \quad (8)$$

where

$$\phi(x,\nabla f)dA = \begin{cases} \frac{1}{q(x)}|\nabla f|^{q(x)}, & |\nabla f| < \beta \\ |\nabla f| - \frac{\beta q(x) - \beta^{q(x)}}{q(x)}, & |\nabla f| \geq \beta \end{cases}$$

where $\beta > 0$ is fixed, and $1 \leq q(x) \leq 2$. The term $q(x)$ is chosen as $q(x) = 1 + \frac{1}{1+k|\nabla G_\sigma * I(x)|^2}$ based on the edge gradients. $I(x)$ is the observed image $g(x)$, $G_\sigma(x) = \frac{1}{\sigma}\exp[-|x|^2/(2\sigma^2)]$ is a Gaussian filter. $k > 0$, $\sigma > 0$ are fixed parameters. The main benefit of this equation is that the local image information are computed as prior information for guiding image diffusion. This functional including two equations are both convex and semi-continuous. This leads to a mathematically sound model for ensuring the global convergence. This equation is extended in a Bayesian estimation based double variational regularization not only for image denoising but also for image deblurring.

3 BAYESIAN ESTIMATION BASED VARIATIONAL IMAGE RESTORATION

Following a Bayesian paradigm, the ideal image f, the PSF h and an observed image g fulfill

$$P(f,h|g) = \frac{p(g|f,h)P(f,h)}{p(g)} \propto p(g|f,h)P(f,h) \quad (9)$$

Based on this form, our goal is to find the optimal estimated image f and the optimal blur kernel h that maximizes the posterior $p(f,h|g)$. $\jmath(f|h,g) = -\log\{p(g|f,h)P(f)\}$ and $\jmath(h|f,g) = -\log\{p(g|f,\ h)P(h)\}$ express that the energy cost $\jmath$ is equivalent to the negative log-likelihood of the data.

The resulting method attempts to minimize double cost functions subject to constraints such as non-negativity conditions of the image and energy preservation of PSFs. The objective of the convergence is to minimize double cost functions by combing the energy function for the estimation of PSFs and images.

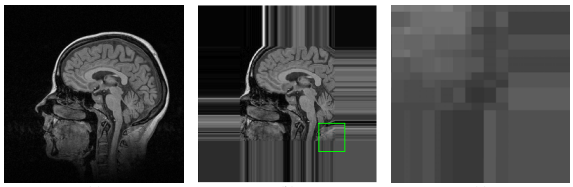

Figure 2: Homogeneous Neumann Boundary Conditions. (a) An original MRI head image. (b)(c) Homogeneous Neumann boundary condition is implemented by mirroring boundary pixels.

We propose a Bayesian based functional on the BV spaces. It is formulated according to

$$\begin{aligned} \jmath_\varepsilon(f,h) &= \frac{\lambda}{2}\int_\Omega (g-hf)^2 dA + \beta\int_\Omega (\nabla h)dA \\ &\quad + \gamma\int_\Omega \phi_\varepsilon(x,Df)dA \end{aligned} \quad (10)$$

The Neumann boundary condition (shown in Fig. 2) $\frac{\partial f}{\partial N}(x,t) = 0$ on $\partial\Omega \times [0,T]$ and the initial condition $f(x,0) = f_0(x) = g$ in Ω are used, where N is the direction perpendicular to the boundary.

3.1 Alternating Minimization

To avoid the scale problem between the minimization of PSF and image via steepest descent, an AM method following the idea of coordinate descent is applied (Zheng and Hellwich, 2006). The AM algorithm decreases complexity.

The equations derived from Eq. (10) are using finite differences which approximate the flow of the Euler-Lagrange equation associated with it,

$$\frac{\partial \jmath_\varepsilon}{\partial f} = \lambda_1 h(-x,-y) * (h * f - g) - \gamma \mathrm{div}(\phi(x,\nabla f))$$

$$\frac{\partial \jmath_\varepsilon}{\partial h} = \lambda_2 f(-x,-y) * (f * h - g) - \beta\nabla h \cdot \mathrm{div}\left(\frac{\nabla h}{|\nabla h|}\right)$$

Neumann boundary conditions are assumed (Acar and Vogel, 1994). In the alternate minimization, blur identification including deconvolution, and data-driven image restoration including denoising are processed alternatingly via the estimation of images and PSFs. The partially recovered PSF is the prior for the next iterative image restoration and vice versa. The algorithm is described in the following:

`Initialization:`
$g(x) = g(x)$, $h_0(x)$ `is random numbers`
`while` *nmse* $>$ *threshold*
(1). *n*th `it.` $f_n(x) = \arg\min(f_n|h_{n-1},g)$,
`fix` $h_{n-1}(x)$, $f(x) > 0$
(2). $(n+1)$th `it.` $h_{n+1} = \arg\min(h_{n+1}|f_n,g)$,
`fix` $f_n(x)$, $h(x) > 0$
`end`

While $h = I$ and I is the identity matrix, the alternating minimization of PSFs and images becomes the estimation of images, e.g., it is corresponding to a denoising problem. While $h \neq I$ (h is generally a convolution operator), it corresponds to a deblurring and denoising problem. The existence and uniqueness of solution remain true, if h satisfies the following hypotheses: (a) h is a continuous and linear operator on $L^2(\Omega)$. (b) h does not annihilate constant functions. (c) h is injective. Thereby, we need to consider the blur kernels at the first step. Further more, we do deconvolution for the blurred noisy image. Then the deconvolved image is smoothed by a family of linear and nonlinear diffusion operators in an alternating minimization.

3.2 Self-Adjusting Regularization Parameters

We have classified the regularization parameters λ in three different levels. Here, we present the method for the selection of window-based regularization parameters λ_w (window w based λ_w, the 1st level). When the size of windows is amplified to the size of an input image, λ becomes a scale regularization parameter for the whole image (the 2nd level). If we fix λ for the whole process, then the selection of regularization parameter is conducted on the level of one fixed λ for the whole process (the 3nd level). We assume that the noise is approximated by additive white Gaussian noise with standard deviation σ to construct a window-based local variance estimation. Then we focus on the adjustment of parameter λ and operators in the smoothing term ϕ. These two computed components can be prior knowledge for preserving discontinuities and detailed textures during image restoration. The Eq. 10 can be formulated in the following,

$$\arg\min \int_\Omega \phi(x, Df(x,y))dA \text{ subject to } \int_\Omega (g-hf)^2 dA$$

where the noise is a Gaussian distributed with variance σ^2. λ can be a Lagrange multiplier in the following form,

$$\lambda = \frac{1}{\sigma^2|\Omega|}\int_\Omega \text{div}\left[\phi(x, Df(x,y))\right](g-hf)dA \quad (11)$$

λ is a regularization parameter controlling the "balance" between the fidelity term and the penalty term. The underlying assumption of this functional satisfies $\|f\|_{BV(\Omega)} = \|f\|_{L^1(\Omega)} + TV(f)$ in the BV space. The distributed derivative $|Df|$ generates an approximation of input "cartoon model"and oscillation model (Meyer, 2001). Therefore, this process preserves discontinuities during the elimination of oscillatory

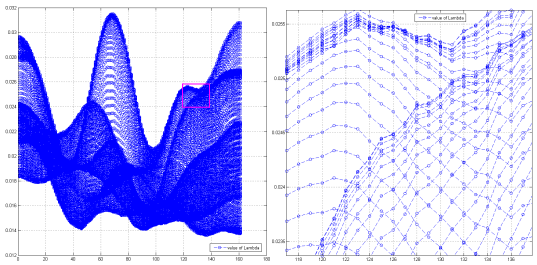

Figure 3: $a|b$. (a) Computed $\lambda \in [0.012, 0.032]$ values in sampling windows for the image with size [160, 160]. (b) Zoom in (a) for showing the distribution of the regularization parameters λ_w.

noise. We note that the term $\int_\Omega (g-hf)^2 dA$ is the power of the residue. Therefore, there exists a relationship among the non-oscillatory sketch "cartoon model" (Mumford and Shah, 1989), (Blake and Zisserman, 1987), oscillation model (Meyer, 2001) and the reduced power of the original image with some proportional measure. We formulate the local variance $L_w(x,y)$ in a given window w based on an input image.

$$L_w(x,y) = \frac{1}{|\Omega|}\int_\Omega [f_w(x,y) - E(f_w)]^2 w(x,y)dxdy \quad (12)$$

where $w(x,y)$ is a normalized and symmetric small window, f_w is the estimated image in a small window w. $E(f_w)$ is the expected value with respect to the window $w(x,y)$ on the size of $\Omega \times \Omega$ estimated image f in each iteration. The local variance in a small window satisfies $var(f_w) = L_w(x,y)$. Thereby, we can write λ for a small window w according to Euler-Lagrange equation for the variation with respect to f Therefore, the regularization equation is with respect to the window-levels. It becomes

$$\jmath_\varepsilon(f) = \sum \lambda_w L_w(x,y) + S_p(f) \quad (13)$$

where $\lambda_w$is a λ in a small window w, $S_p(f)$ is the smoothing term. Thus, we can easily get many λ_w for moving windows which can be adjusted by local variances, shown in Fig. 3. These λ_w are directly used as regularization parameters for adjusting the balance during the energy optimization. They also adjust the strength of diffusion operators for keeping more fidelity during the diffusion process. The related regularization parameters β and γ incorporate the λ, while the parameter λ of the fidelity term needs to be defined.

During image restoration, the parameter λ can be switched among three different levels. The window-based parameter λ_w and the scale-based (entire image) parameter can be adjusted to find the optimal results. Simultaneously, λ thus control the image fidelity and diffusion strength of each selected operator in an optimal manner.

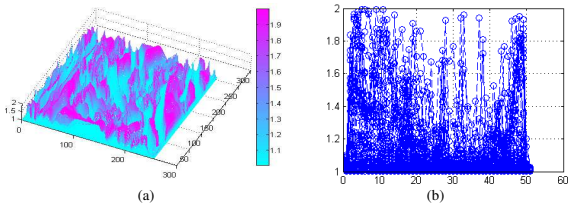

Figure 4: Strength of $p(x)$ in the Lena image. (a) Strength of $p(x)$ between [1,2] in the Lena image. (b) Strength of $p(x)$ is shown in a cropped image with size $[50,50]$.

3.3 Data-Driven Image Diffusion

The numerical implementation is crucial for the algorithm. The data-driven diffusion term $\mathrm{div}(\phi(a,\nabla f))$ can be numerically approximated in the following,

$$\mathrm{div}(\phi(x,\nabla f)) = \underbrace{|\nabla f|^{p(x)-2}}_{\text{Coefficient}}\underbrace{[(p(x)-1)\Delta f}_{\text{IsotropicTerm}}$$
$$+\underbrace{(2-p(x))|\nabla f| div(\frac{\nabla f}{|\nabla f|})}_{\text{CurvatureTerm}}+\underbrace{\nabla p\cdot\nabla f\log|\nabla f|]}_{\text{HyperbolicTerm}}$$

with

$$p(x)=\begin{cases} q(x)\equiv 1+\frac{1}{1+k|\nabla G_\sigma * I(x)|^2}, & |\nabla f|<\beta \\ 1, & |\nabla f|\geq\beta \end{cases}$$

We indicate with div the divergence operator, and with ∇ and Δ respectively the gradient and Laplacian operators, with respect to the space variables. The numerical implementation of the nonlinear diffusion operator is based on *central differences* for coefficient and the isotropic term, *minmod scheme* for the curvature term, and *upwind finite difference scheme* in the seminal work of Osher and Sethian for curve evolution (Rudin et al., 1992) of the hyperbolic term based on the hyperbolic conservation laws. We use here the minmod function, in order to reduce the oscillations and to get the correct values of derivatives in the case of local maxima and minima.

The image is restored by denoising in the process of edge-driven image diffusion as well as deblurring in the process of image deconvolution. Firstly, the chosen variable exponent of $p(x)$ is based on the computation of gradient edges in the image, shown in Fig. 4. In homogeneous flat regions, the differences of intensity between neighboring pixels are small; then the gradient ∇G_σ become smaller ($p(x)\to 2$). The isotropic diffusion operator (Laplace) is used in such regions. In non-homogeneous regions (near a edge or discontinuity), the anisotropic diffusion filter is chosen continuously based on the gradient values ($1<p(x)<2$) of edges. The reason is that the discrete chosen anisotropic operators will hamper the recovery of edges (Nikolova, 2004). Secondly, the nonlinear diffusion operator for piecewise image smoothing is processed during image deconvolution based on a previously estimated PSF. Finally, coupling estimation of PSF (deconvolution) and estimation of image (edge-driven piecewise smoothing) are alternately optimized applying a stopping criteria. Hence, over-regularization or under-regularization is avoided by pixels at the boundary of the restored image.

4 NUMERICAL EXPERIMENTS

Experiments on synthetic and real data are carried out to demonstrate the effectiveness of this algorithm.

Effects of different types and strengths of noise and blur. Firstly, we test the suggested method in different degraded data. Fig. 6 shows that the image denoising and deblurring can be successfully achieved even on the very strong noise level $SNR = 1.5dB$. In this figure, we can observe that the number of iteration is dependent on the strength of noise. If the noise is stronger, the number of iteration becomes larger. Fig. 7 shows that the suggested approach on the BV space is robust for different types of noise. The impulsive noise with different strengths can also be successfully eliminated, while structure and main textures are still preserved. We have also tested this approach in different types of noise, speckle, impulsive, Poisson, Gaussian noise in different levels, shown in Fig. 8.

Comparison with other methods. Secondly, we have compared the TV method with two types of conditions. From visual perception and denoising viewpoint, our method favorably compares to some state-of-the-art methods: the TV method (Rudin et al., 1992) and a wavelet method (Portilla et al., 2003). In Fig. 5, the structure of the restored fingerprint is largely enhanced than the original image in our method and more recognizable in comparison with the restored image using the GSM method (Portilla et al., 2003).

Table 1: ISNR (dB) Results on Test Data.

SNR	TV-fixed λ	TV- adaptive λ	Our met.
13.8	15.39	17.85	19.16
12.5	14.42	17.12	18.14
8.7	11.58	15.03	16.26
8.6	11.34	15.02	16.09

Table 1 shows the different properties of different methods. Although our method does not have significant improvement on the value of ISNR (dB) in Table 1, the measure of ISNR can not fully measure human visual perception. Our method really achieves high-fidelity and visual smoothness than the

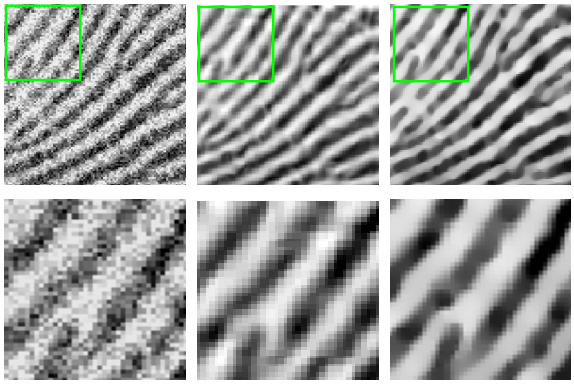

Figure 5: $\frac{a|b|c}{d|e|f}$. Comparison of two methods for fingerprint denoising. (a)(d) Cropped noisy image, $SNR = 8$ dB. (b)(e) GSM method (Portilla et al., 2003) PSNR=27.8. dB. (c)(f) The suggested method PSNR= 28.6 dB.

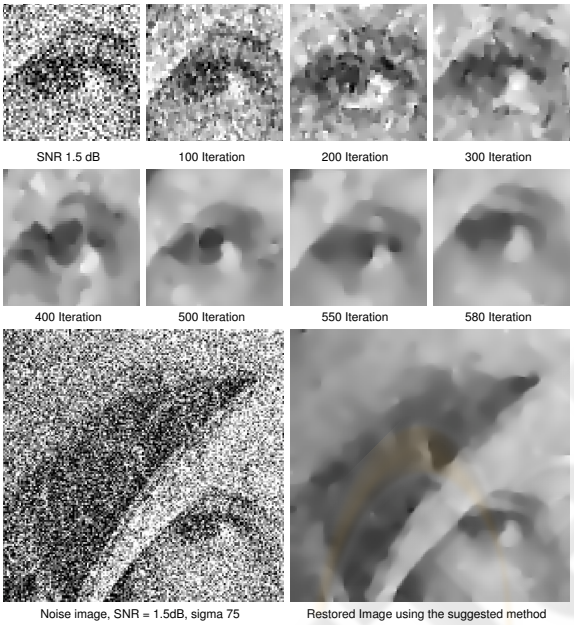

Figure 6: Restored image using the suggested method. Stronger distributed noise with $SNR = 1.5dB$. 100 iterations need 600 seconds for the image size of [512,512].

TV methods. The TV methods with fixed λ and adaptive λ still have some piecewise constant effects on restored images. Furthermore, our method keeps high-fidelity for restoring stronger or impulsive noisy images, while the TV methods (fixed λ and adaptive λ) cannot keep high-fidelity for restoring such degraded images, e.g., SNR = 1.5dB or some impulsive noisy images, shown in Fig. 6, Fig. 7 and Fig. 8.

More results are shown in Fig. 9 to demonstrate that the suggested method keeps high-fidelity and visual perception image restoration. These experiments show that the suggested method on the BV space has some advantages on image denoising and image restoration. It can also be easily extended to other related early vision problems.

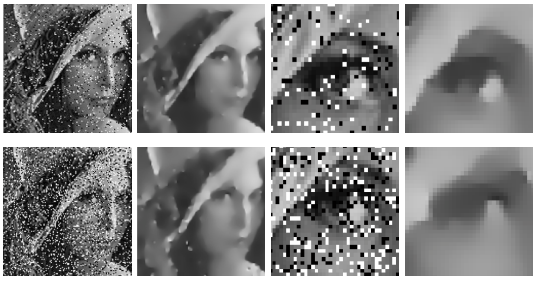

Figure 7: $\frac{a|b|c|d}{e|f|g|h}$. Restoration of impulsive noise images. (a) 10% salt-pepper noise image. (b) Restored image, 200 iterations. (c)(d) Zoom in images from (a)(b) respectively. (e)25% salt-pepper noise image. (f) Restored image, 900 iterations. (g)(h) Zoom in images from (e)(f) respectively.

Figure 8: $\frac{a|b|c|d}{e|f|g|h}$. Image denoising using the suggested method. (a)(b)Speckle noise image and denoising. (c)(d) Zoom in from (a)(b) respectively, 100 iterations. (e)(f) Poisson noise image and denoising. (g)(h) Zoom in from (e)(f) respectively, 100 iteration.

5 CONCLUSION

The main structure and skeleton of images are well approximated on the BV space. In order to preserve textures and detailed structures, more constraints or generative prior information are investigated. We have developed a self-adjusting scheme that controls the image restoration based on the edge-driven convex semi-continuous functionals. The performance of image restoration is not only based on the computed gradient but also based on local variances of the residues. Therefore, linear and nonlinear smoothing operators in the smoothing term are continuously self-adjusting via the gradient power. The consistency of self-adjusting local variances and the global convergence can be achieved in the iterative convex optimization approach. We have shown that this algorithm has relatively robust performance for different types and strengths of noise. The image restoration keeps high fidelity to the original image.

(a) (b) (c)

Figure 9: Image denoising using the suggested method. (a) column: Original images. (b) column: Noisy images with SNR = 10 dB . (c) column: Restored images (100 iterations) using the suggested method.

REFERENCES

Acar, R. and Vogel, C. R. (1994). Analysis of bounded varaition penalty methods for ill-posed problems. *Inverse problems*, 10(6):1217–1229.

Alvarez, L. and Gousseau, Y. (1999). Scales in natural images and a consequence on their bounded variation norm. In *Scale-Space*, volume Lectures Notes on Computer Science, 1682.

Aubert, l. and Vese, L. (1997). A variational method in image recovery. *SIAM Journal Numer. Anal.*, 34(5):1948–1979.

Blake, A. and Zisserman, A. (1987). *Visual Reconstruction*. MIT Press, Cambridge.

Chambolle, A. and Lions, P. L. (1997). Image recovery via total variation minimization and related problems. *Numer. Math.*, 76(2):167–188.

Chan, T. F., Kang, S. H., and Shen, J. (2002). Euler's elastica and curvature based inpaintings. *SIAM J. Appli. Math*, pages 564–592.

Chan, T. F. and Shen, J. (2006). Theory and computation of variational image deblurring. *Lecture Notes on "Mathematics and Computation in Imaging Science and Information Processing"*.

Chen, Y., Levine, S., and Rao, M. (2006). Variable exponent, linear growth functionals in image restoration. *SIAM Journal of Applied Mathematics*, 66(4):1383–1406.

Chen, Y. and Rao, M. (2003). Minimization problems and associated flows related to weighted *p* energy and total variation. *SIAM Journal of Applied Mathematics*, 34:1084–1104.

Demengel, F. and Teman, R. (1984). Convex functions of a measure and applications. *Indiana University Mathematics Journal*, 33:673–709.

Freeman, W. and Pasztor, E. (2000). Learning low-level vision. In Academic, K., editor, *International Journal of Computer Vision*, volume 40, pages 24–57.

Geman, S. and Reynolds, G. (1992). Constrained restoration and the recovery of discontinuities. *IEEE Trans. PAMI.*, 14:367–383.

Giusti, E. (1984). *Minimal Surfaces and Functions of Bounded Variation*. Birkhäuser.

Goffman, C. and Serrin, J. (1964). Sublinear functions of measures and variational integrals. *Duke Math. J.*, 31:159–178.

Gousseau, Y. and Morel, J.-M. (2001). Are natural images of bounded variation? *SIAM Journal on Mathematical Analysis*, 33:634–648.

Meyer, Y. (2001). Oscillating patterns in image processing and in some nonlinear evolution equations. *The 15th Dean Jacquelines B. Lewis Memorial Lectures*, 3.

Mumford, D. and Shah, J. (1989). Optimal approximations by piecewise smooth functions and associated variational problems. *Communications on Pure and Applied Mathematics*, 42:577–684.

Nikolova, M. (2004). Weakly constrained minimization: application to the estimation of images and signals involving constant regions. *J. Math. Image Vision*, 21(2):155–175.

Portilla, J., Strela, V., Wainwright, M., and Simoncelli, E. (2003). Image denoising using scale mixtures of Gaussians in the Wavelet domain. *IEEE Trans. on Image Processing*, 12(11):1338–1351.

Rudin, L., Osher, S., and Fatemi, E. (1992). Nonlinear total varition based noise removal algorithm. *Physica D*, 60:259–268.

Vese, L. A. (2001). A study in the BV space of a denoising-deblurring variational problem. *Applied Methematics and Optimization*, 44:131–161.

Weickert, J. and Schnörr, C. (2001). A theoretical framework for convex regularizers in PDE-based computation of image motion. *International Journal of Computer Vision*, 45(3):245–264.

Zheng, H. and Hellwich, O. (2006). Double regularized Bayesian estimation for blur identification in video sequences. In *P.J. Narayanan et al. (Eds.) ACCV*, volume 3852 of *LNCS*, pages 943–952. Springer.